Boron nitride encapsulated graphene infrared emitters

H. R. Barnard, E. Zossimova, N. H. Mahlmeister, L. M. Lawton, I. J. Luxmoore, and G. R. Nash

Citation: Applied Physics Letters **108**, 131110 (2016); doi: 10.1063/1.4945371
View online: http://dx.doi.org/10.1063/1.4945371
View Table of Contents: http://scitation.aip.org/content/aip/journal/apl/108/13?ver=pdfcov
Published by the AIP Publishing

Boron nitride encapsulated graphene infrared emitters

H. R. Barnard, E. Zossimova, N. H. Mahlmeister, L. M. Lawton, I. J. Luxmoore, and G. R. Nash[a)]
College of Engineering, Mathematics and Physical Sciences, University of Exeter, Exeter EX4 4QF, United Kingdom

(Received 19 January 2016; accepted 23 March 2016; published online 31 March 2016)

The spatial and spectral characteristics of mid-infrared thermal emission from devices containing a large area multilayer graphene layer, encapsulated using hexagonal boron nitride, have been investigated. The devices were run continuously in air for over 1000 h, with the emission spectrum covering the absorption bands of many important gases. An approximate solution to the heat equation was used to simulate the measured emission profile across the devices yielding an estimated value of the characteristic length, which defines the exponential rise/fall of the temperature profile across the device, of 40 μm. This is much larger than values obtained in smaller exfoliated graphene devices and reflects the device geometry, and the increase in lateral heat conduction within the devices due to the multilayer graphene and boron nitride layers. © *2016 AIP Publishing LLC*.
[http://dx.doi.org/10.1063/1.4945371]

There is a continuing need for the development of new infrared (IR) light sources to enable low cost, intrinsically safe, portable gas sensors for applications such as emissions monitoring. Most existing IR sensors use conventional incandescent sources which have several shortcomings including slow response time, limited wavelength range (due to the glass envelope of the source), and limited lifetimes due to the fragility of the source. Silicon based micro-machined heaters[1] have the advantage of being CMOS compatible, but still have a relatively slow response time (maximum modulation frequencies of ~100 Hz), limiting the response of the sensor and implementation of advanced signal processing techniques. Semiconductor LEDs (light-emitting-diodes)[2] offer a natural route for the replacement of conventional incandescent sources, but devices with the narrow bandgap required to achieve emission at the relatively long wavelengths required for the sensing of many important gases, such as NOx, suffer both from relatively poor internal[3] and external quantum efficiencies,[4] leading to relatively low overall efficiencies. For example, the room temperature wall-plug efficiency (WPE), the ratio of the electrical power in to the optical power out, of the $Al_xIn_{1-x}Sb$ based LEDs described by Nash *et al.*[2] was approximately 0.02%. A much higher WPE of 0.15% has recently been reported in interband cascade devices with peak emission at 3.3 μm,[5] but this is still much lower than in LEDs operating at shorter wavelengths. These semiconductor LEDs also typically incorporate elements such as indium and gallium, for which there are concerns regarding sustainability, and require the precise epitaxial growth of a large number of layers.

Although there has been much recent interest[6,7] in the use of graphene as an incandescent source emitting in the visible, infrared thermal emission has primarily been used as a means of probing the electronic structure of monolayer graphene transistor devices under bias.[9–13] Nevertheless, several of graphene's remarkable properties do make it attractive for the realization of an infrared incandescent source. For example, it is able to sustain extremely large current densities: 10^7 A/cm^2 in micron sized wires fabricated from graphene grown by chemical vapor deposition (CVD),[8] compared to values of ~100 A/cm^2 in a conventional tungsten filament light bulb. Its low thermal mass (approximately three orders of magnitude smaller even than a typical silicon cantilever) offers the prospect for high frequency operation, and we have recently assessed the potential of using graphene based thermal emitters as an alternative, less complicated, approach to semiconductor LEDs.[14,15] For the currents used, the emission from these devices peaked at a wavelength of around 4 μm and a measureable modulation of the emission was observed up to a drive frequency of 100 kHz, much higher than in silicon based micro-heaters. However, these devices only operated in vacuum, and in this paper we demonstrate the use of hexagonal boron nitride (h-BN) as a means of encapsulating the emitting area, allowing sustained operation in air, and investigate how the incorporation of the h-BN layers modifies the thermal properties of the devices.

Devices consisting of multilayer graphene encapsulated between two layers of multilayer h-BN were fabricated using 13 nm thick multilayer h-BN on Cu, from Graphene Supermarket, and 6–8 layer multilayer graphene on polymer, from ACS. Note that the choice of the 6–8 layer graphene and 13 nm h-BN was motivated by the availability of these materials from the manufacturers, together with our experience of handling different thickness layers, but that the type and thickness of the layers has not yet been optimized. The graphene and h-BN were transferred, using the standard process,[16] onto a heavily doped silicon wafer capped with 300 nm of SiO_2. Prior to the removal of the Cu layer, with a 0.1 mol concentration of ammonium persulphate for 12 h, a thin 80 nm layer of neat A6 950 K PMMA was spun onto the h-BN and baked for 8 min. After etching, the materials were rinsed in six fresh DI water solutions over a period of 48 h, before transfer onto the substrate using a glass spoon. The

a)Author to whom correspondence should be addressed. Electronic mail: g.r.nash@exeter.ac.uk

six step device fabrication is illustrated schematically in Figure 1: (a) the initial transfer of multilayer h-BN, followed by lithography and dry etching to define a 600 μm × 500 μm^2; (b) the transfer and definition, through lithography and a second dry etching step, of an overlaying area of multilayer graphene; (c) definition of a 50 μm × 600 μm area of 50 nm thick gold onto the outer edges of the multilayer graphene for improved contact resistance; (d) definition of areas of 100 μm × 600 μm of 7 nm/70 nm Cr/Au onto the Au and Si/SiO_2 to ensure good contact with the final contact layer after encapsulation; (e) the transfer and definition, via lithography and a final dry etching step, of the final encapsulating h-BN layer; (f) definition of final 7 nm/70 nm Cr/Au contacts over the prior 100 μm × 600 μm Cr/Au metallization, and extended over the chip to provide 200 μm × 200 μm pads for bonding; (g) microscopic image of a completed device. Note that the final metallization step not only defines the bond pads but also acts to provide mechanical and thermal anchoring of the top h-BN layer. The devices were mounted on ceramic chip holders and all measurements were performed at ambient temperature and in air. Two terminal current-voltage measurements were made, with the values of resistances obtained (~1000 Ω) typical of those obtained from CVD graphene.[17] The thermal emission from the devices was collected using a 15× reflecting objective lens (numerical aperture = 0.28) which was mounted on a xy-stage so that it could be scanned over the device. Light from the reflecting objective passed through a mirror system and was then focused, using a CaF_2 lens, onto the entrance of a Jobin-Yvon iHR550 grating spectrometer. The spectrometer was equipped with a turret system so that the collected light was incident either on a mirror for mapping measurements, or a 4 μm blazed diffraction grating for spectral measurements, before being focused onto a liquid nitrogen cooled HgCdTe detector, with a 2–12 μm response. The devices were driven by a 1 kHz square waveform (50% duty cycle), using a Keithley 6221 current source, at peak injection currents of tens of milliamps. The signal from the detector was amplified by a low noise preamplifier and passed to a lock-in amplifier for phase sensitive measurement. Measurements are presented from one device, but similar behavior was observed from a second device. At the time of writing, the second device has been running continuously in air, with current of 100 mA, for well over 1000 h.

The measured spatial variation of the thermal emission for a peak current of 50 mA is shown in Figure 2(a). In

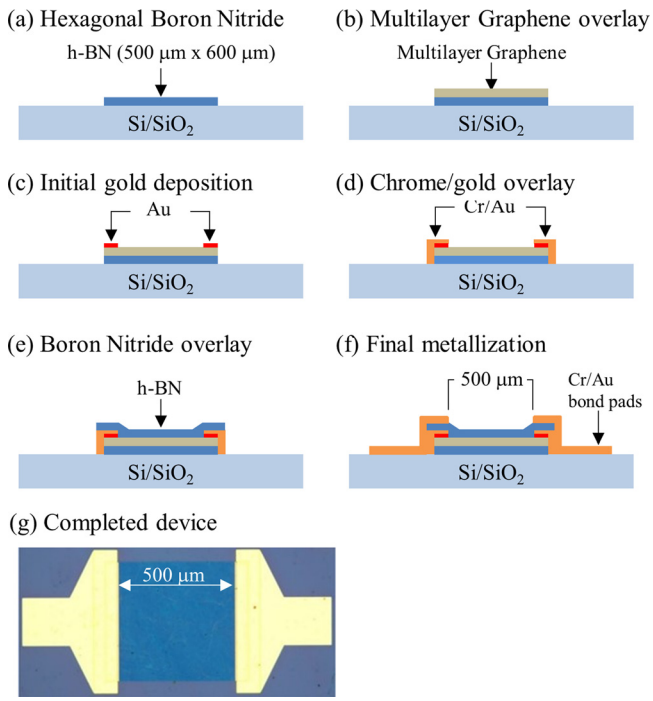

FIG. 1. Schematic cross-section diagram illustrating the device fabrication: (a) initial h-BN layer on Si/SiO_2 chip, (b) multilayer graphene overlay, (c) 50 nm thick Au deposited on the edges of multilayer graphene, (d) initial 7 nm/70 nm thick Cr/Au layer deposited on Au and Si/SiO_2 chip, (e) encapsulating h-BN layer on multilayer graphene and inner edges of initial Cr/Au layer, (f) final contact layer of 7 nm/70 nm Cr/Au on initial Cr/Au layer and edges of encapsulating BN layer, and (g) microscope image of a completed device.

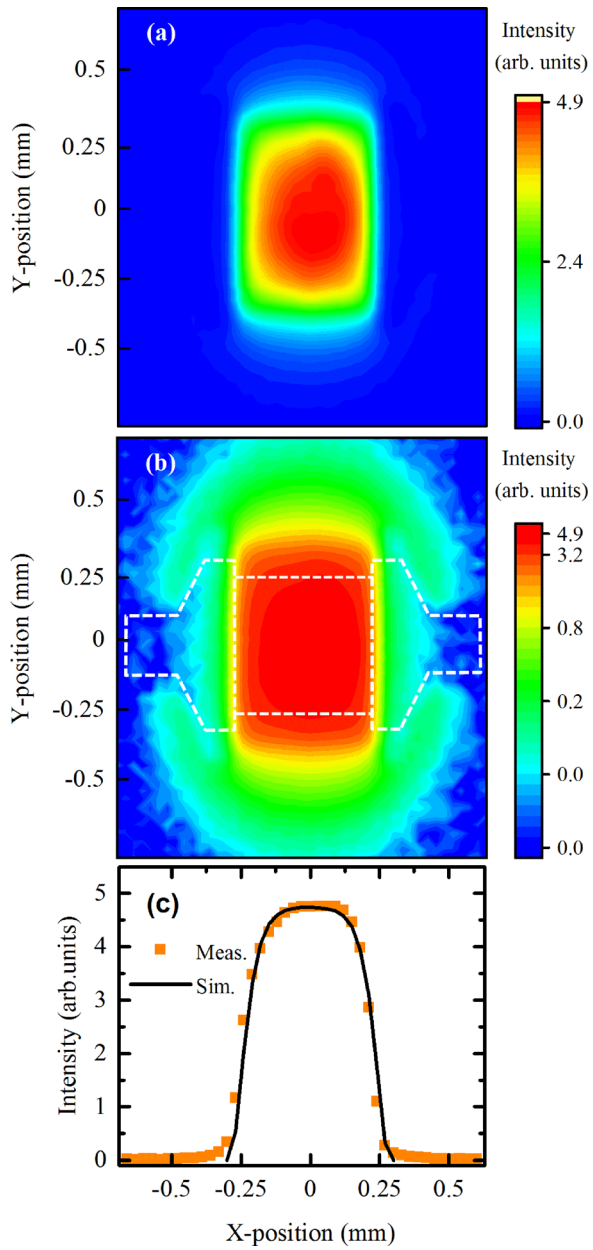

FIG. 2. (a) Thermal emission mapped for a peak current of 50 mA; (b) same data plotted on a logarithmic vertical scale; and (c) variation of the measured intensity as a function of X-position, where the symbols correspond to the measured data and the line to the simulated profile. The white dotted lines in (b) indicate the position of the metal contacts and multilayer graphene.

contrast to monolayer graphene based devices, the thermal emission has a maximum intensity in the center of the emitting area, as might be expected from a conventional semimetal filament. Figure 2(b) shows the same data plotted on a logarithmic vertical scale, where the dotted white lines indicate the orientation and approximate position of the device. It can be seen that there is much less emission from the area of the metal contacts than from the graphene emitter area, suggesting that the metal contacts do not get significantly hot and act to thermally anchor the device in the x-direction. In the y-direction, the emission extends over a much larger area suggesting that there is significant lateral diffusion of the heat generated in the graphene. In Figure 2(c), the measured emission is plotted as function of x-position, for $y = 0$, and shows that the emission is fairly constant in the center of the device and falls to near zero at the metal contacts, behavior typical of a relatively long conventional filament supported by two colder supports. The profile of the temperature, T, along the x-direction can be approximated by the following steady-state heat equation

$$-hwk\frac{d^2T}{dx^2} + g(T - T_0) + w\varepsilon\sigma T^4 = \frac{I^2R}{L}, \quad (1)$$

where w, h, and L are the width, height, and length of the thermally conducting channel, respectively (note that heat loss through convection is assumed to be much smaller than that through conduction). The term on the right hand side of Equation (1) corresponds to the heat generated per unit length through Joule heating, where I is the current and R the resistance of the device (assuming uniform heat generation along the conducting channel). The first term on the left-hand-side of the equation is the heat lost through diffusion, where k is the lateral thermal conductivity, whereas the middle term of the left-hand-side of Equation (1) represents the heat lost vertically to the underlying substrate, which is assumed to be at a temperature $T_0 \ll T$, and where g is the net heat loss rate to the substrate per unit length.[18] The third term on the left-hand-side of the equation corresponds to the heat lost through radiation per unit length, where σ is the Stefan–Boltzmann constant and ε is the emissivity of the emitting area. The emissivity of monolayer graphene has been previously measured as $1.6 \pm 0.8\%$,[11] in good agreement with the accepted value of the absorbance. In a multilayer device, the emissivity is expected to increase linearly with the number of layers,[14] as with the absorbance,[19] and in the devices studied here (which have 6–8 layers) the emissivity of the multilayer graphene is expected to be ~10%. Heat loss through radiation is therefore also assumed to be smaller than that lost through diffusion and an approximate solution to Equation (1) is given then by[20]

$$T(x) = T_{\max}\left[1 - \frac{\cosh(x/\lambda)}{\cosh(L/2\lambda)}\right] \text{ for } -L/2 < x < L/2, \quad (2)$$

where $T_{\max}$ is the peak temperature in the center of the device, and where λ is a characteristic length that defines the exponential rise/fall of the temperature profile (heat generated within a distance of λ from the contacts will flow through the graphene to the contacts) and is given by: $\lambda = (kA/g)^{\frac{1}{2}}$. Finally, the measured emission is assumed to be proportional to T^4 as graphene is known to be a grey-body.[14] The line shown in Figure 2(c) was calculated using Equation (2) to obtain the temperature profile, and then by varying λ to give the best fit to the measured data, yielding a characteristic length of 40 μm. This is two orders of magnitude larger than typical values, 0.1–0.2 μm, obtained from exfoliated graphene devices on SiO_2 substrates,[9] but reflects the effects of the multilayer graphene, the h-BN and the device geometry in these devices. This can be understood by first considering the heat loss rate to the substrate, g, which is approximately given by

$$g \approx \frac{1}{L(R_{ox} + R_{BN} + R_{Si})}, \quad (3)$$

where the thermal resistance of the silicon oxide can be written as $R_{ox} = t_{ox}/(k_{ox}wL) \approx 1$ K/W, where $t_{ox} \approx 300$ nm and $k_{ox} \approx 1.4$ W m^{-1} K^{-1} are the thickness and thermal conductively, respectively, of the SiO_2.[9] The vertical thermal resistance of the bottom h-BN layer can likewise be written as $R_{BN} = t_{BN}/(k_{BN}wL) \approx 0.03$ K/W, with $t_{BN} \approx 13$ nm and $k_{BN} \approx 2$ W m^{-1} K^{-1}.[21] The thermal resistance into the silicon wafer $R_{Si} = 1/[2k_{Si}(wL)^{1/2}] \approx 20$ K/W,[8] where $k_{ox} \approx 50$ W m^{-1} K^{-1}, leading to a total heat loss into the substrate, per unit length, $g \approx 96$ W K^{-1} m^{-1}, larger than in smaller exfoliated devices. However, as the basal plane (lateral) thermal conductivity of the boron nitride, ~400 W m^{-1} K^{-1} at room temperature,[22] is similar to that of the graphene, the presence of the two h-BN layers increases the thickness h of the thermally conducting lateral channel. Taking the combined thickness of the graphene and two h-BN layers to be ~30 nm, with an effective thermal conductivity of ~500 W m^{-1} K^{-1}, yields a value of λ of approximately 10 μm, which is consistent with the value obtained experimentally in this work. In this simple analysis, we have ignored the extra vertical thermal resistance caused by the interfaces between the different layers, and also any effect due to the possible wrinkling of the 2D materials, both of which could act to increase the thermal resistance into the substrate thus increasing λ. In contrast, residues from the transfer process have been shown to decrease the lateral thermal conductivity of h-BN,[23] which would decrease the characteristic length. Although a full study of the dominant contributions to the overall thermal characteristics of the devices, including the effects of heat loss through radiation, convection, and via the contacts, is beyond the scope of this manuscript, this simple analysis highlights the potential of this architecture to be used to engineer the thermal properties of these devices to, for example, maximize the difference between the "on" and "off" temperatures of the emitting area.

The uncorrected emission spectrum, measured at the center of the device, is shown as a function of current in Figure 3(a), where the large minimum in measured intensity at a wavelength of 4.2 μm is due to absorption by atmospheric CO_2. As the current is increased, the peak emission moves to shorter wavelengths and the integrated emission increases. To correct for the efficiency of the spectrometer grating, the detector response, and absorption by CO_2 and water in the atmosphere, the measurements were calibrated

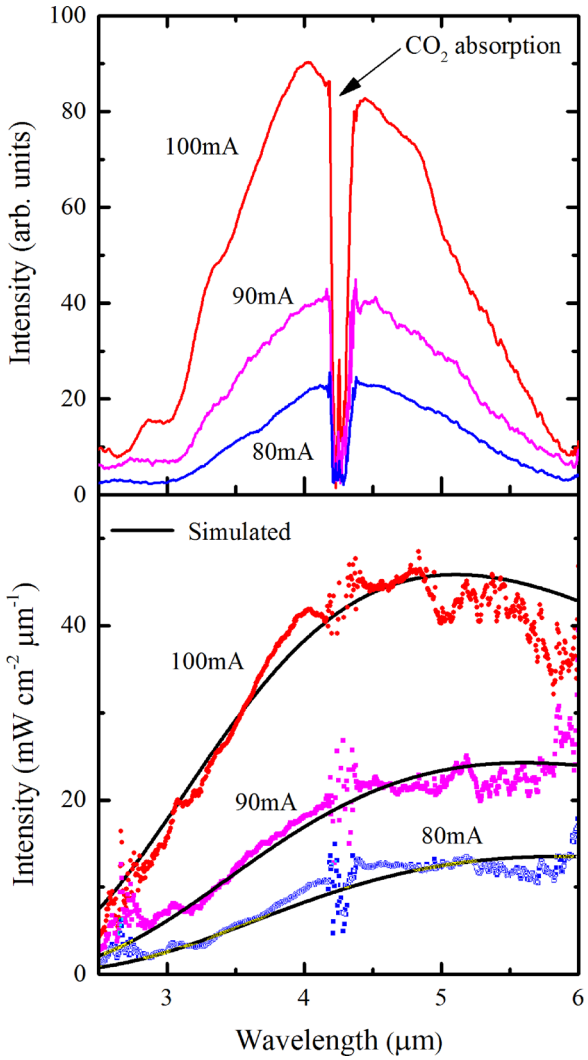

FIG. 3. (a) Measured raw emission spectra as a function of peak current and (b) corrected emission spectra (symbols) together with simulated spectra (lines).

using a 673 K blackbody source and the corrected spectra are shown in Figure 3(b). The emission can be seen to cover the characteristic absorption of many important gases, including carbon dioxide and nitric oxide. An indication of the temperature of the surface of the device can be made by assuming that the measured spectra corresponds to the difference between two grey-body curves, one corresponding to emission when the current is on, and the second corresponding to emission from a cooler grey-body when the current is. The lines shown in Figure 3(b) were obtained by calculating the difference between two grey-body curves, with the emissivity in both cases assumed to be 10% and the "on" and "off" temperatures taken to give the best qualitative fit to the corrected spectra. This yielded "on" and "off" temperatures of 530 K and 390 K, 475 K and 375 K, and 440 K and 370 K for currents of 100 mA, 90 mA, and 80 mA, respectively. These temperatures are broadly equivalent to those we have measured previously using devices without encapsulation in vacuum and suggest that with relatively long current pulses the devices reach the same equilibrium state in both cases. However, the measured intensity at high frequencies is more in encapsulated devices compared to devices without the encapsulation.[15] In addition, the second device to be tested has been running continuously in air, with a drive current of 100 mA, for well over 1000 h at the time of writing, in contrast to similar devices without boron nitride encapsulation, which typically only operate for a few minutes in air. A full study of the device failure mechanisms, which are thought to be similar to those of conventional filaments, is beyond the scope of the work presented here, but the h-BN appears to effectively isolate the multilayer graphene layer from air and may also lead to a more uniform heating of the device. Finally, the electrically insulating top surface provided by the h-BN also means these devices provide a platform for the future integration of photonic structures[24] designed to tailor the emission for gas sensing applications.

In conclusion, we have investigated the spatial and spectral characteristics of mid-infrared thermal emission from devices containing a multilayer graphene layer encapsulated using hexagonal boron nitride. An approximate solution to the heat equation was used to simulate the measured emission profile across the devices yielding an estimated value of the characteristic length, which defines the exponential rise/fall of the temperature profile across the device, of 40 μm. This is much larger than values obtained in exfoliated graphene devices and reflects the increase in the lateral thermal conductivity caused by the use of multilayer graphene, boron nitride encapsulation, and the device geometry. Finally, the devices are able to operate continuously in air for over 1000 h, with the emission spectrum covering the characteristic absorption of many important gases.

This work has been undertaken as part of an UK Engineering and Physical Sciences Research Council Fellowship (GRN) in Frontier Manufacturing (Grant No. EP/J018651/1).

[1]See S. Z. Ali, A. De Luca, R. Hopper, S. Boual, J. Gardner, and F. Udrea, IEEE Sens. J. **15**, 6775 (2015); and references therein.
[2]See, for example, N. V. Zotova, N. D. Il'inskaya, S. A. Karandashev, B. A. Matveev, M. A. Remennyi, and N. M. Stus', Semiconductors **40**, 697 (2006); M. K. Haigh, G. R. Nash, S. J. Smith, L. Buckle, M. T. Emeny, and T. Ashley, Appl. Phys. Lett. **90**, 231116 (2007); G. R. Nash, H. L. Forman, S. J. Smith, P. B. Robinson, L. Buckle, S. D. Coomber, M. T. Emeny, N. T. Gordon, and T. Ashley, IEEE Sens. J. **9**, 1240 (2009); K. J. Cheetham, A. Krier, I. P. Marko, A. Aldukhayel, and S. J. Sweeney, Appl. Phys. Lett. **99**, 141110 (2011).
[3]B. I. Mirza, G. R. Nash, S. J. Smith, L. Buckle, S. D. Coomber, M. T. Emeny, and T. Ashley, J. Appl. Phys. **104**, 063113 (2008).
[4]I. J. Buss, G. R. Nash, J. G. Rarity, and M. J. Cryan, J. Opt. Soc. Am. B. **25**, 810 (2008).
[5]J. Abell, C. S. Kim, W. W. Bewley, C. D. Merritt, C. L. Canedy, I. Vurgaftman, J. R. Meyer, and M. Kim, Appl. Phys. Lett. **104**, 261103 (2014).
[6]D. Yu and L. Dai, Appl. Phys. Lett. **96**, 143107 (2010).
[7]Y. D. Kim, H. Kim, Y. Cho, J. H. Ryoo, C.-H. Park, P. Kim, Y. S. Kim, S. Lee, Y. Li, S.-N. Park, Y. S. Yoo, D. Yoon, V. E. Dorgan, E. Pop, T. F. Heinz, J. Hone, S.-H. Chun, H. Cheong, S. W. Lee, M.-H. Bae, and Y. D. Park, Nat. Nanotechnol. **10**, 676 (2015).
[8]K.-J. Lee, A. P. Chandrakasan, and J. Kong, Electron Device Lett. **32**, 557 (2011).
[9]M. Bae, Z. Ong, D. Estrada, and E. Pop, Nano Lett. **10**, 4787 (2010).
[10]M. H. Bae, S. Islam, V. E. Dorgan, and E. Pop, ACS Nano **5**, 7936 (2011).
[11]M. Freitag, H.-Y. Chiu, M. Steiner, V. Perebeinos, and P. Avouris, Nat. Nanotechnol. **5**, 497 (2010).
[12]K. L. Grosse, M. H. Bae, F. Lian, E. Pop, and W. P. King, Nat. Nanotechnol. **6**, 287 (2011).

[13]I. J. Luxmoore, C. Adlem, T. Poole, L. M. Lawton, N. H. Mahlmeister, and G. R. Nash, Appl. Phys. Lett. **103**, 131906 (2013).
[14]L. M. Lawton, N. H. Mahlmeister, I. J. Luxmoore, and G. R. Nash, AIP Adv. **4**, 087139 (2014).
[15]N. H. Mahlmeister, L. M. Lawton, I. J. Luxmoore, and G. R. Nash, Appl. Phys. Express **9**, 012105 (2016).
[16]X. Li, W. Cai, J. An, S. Kim, J. Nah, D. Yang, R. Piner, A. Velamakanni, I. Jung, E. Tutuc, S. K. Banerjee, L. Colombo, and R. S. Ruoff, Science **324**, 1312 (2009).
[17]X. Li, Y. Zhu, W. Cai, M. Borysiak, B. Han, D. Chen, R. D. Piner, L. Colombo, and R. S. Ruoff, Nano Lett. **9**, 4359 (2009).
[18]E. Pop, D. A. Mann, K. Goodson, and H. Dai, J. Appl. Phys. **101**, 093710 (2007).
[19]Q. Bao, H. Zhang, Y. Wang, Z. Ni, Y. Yan, Z. X. Shen, K. P. Loh, and D. Y. Tang, Adv. Funct. Mater **19**, 3077 (2009).
[20]E. Pop, Nano Res. **3**, 147 (2010).
[21]A. Simpson and A. D. Stuckes, J. Phys. C: Solid State Phys. **4**, 1710 (1971).
[22]E. K. Sichel, R. E. Miller, M. S. Abrahams, and C. J. Buiocchi, Phys. Rev. B **13**, 4607 (1976).
[23]I. Jo, M. T. Pettes, J. Kim, K. Watanabe, T. Taniguchi, Z. Yao, and L. Shi, Nano Lett. **13**, 550 (2013).
[24]See, for example, P. Q. Liu, I. J. Luxmoore, S. A. Mikhailov, N. A. Savostianova, F. Valmorra, J. Faist, and G. R. Nash, Nat. Commun. **6**, 8969 (2015).